ACS OMEGA

http://pubs.acs.org/journal/acsodf

Article

Utilizing the Oxygen Reduction Reaction in Particle Impact Electrochemistry: A Step toward Mediator-Free Digital Electrochemical Sensors

Taghi Moazzenzade, Jurriaan Huskens, and Serge G. Lemay*

Cite This: *ACS Omega* 2023, 8, 31265−31270

Read Online

ACCESS | Metrics & More | Article Recommendations | Supporting Information

ABSTRACT: The current blockade particle impact method opens a route toward highly parallelized single-entity electrochemical assays. An important limitation is, however, that a redox mediator must be present in the sample, which can detrimentally interfere with molecular recognition processes. Dissolved O_2 that is naturally present in aqueous solutions under ambient conditions can in principle serve as a suitable mediator via the oxygen reduction reaction (ORR). Here, we demonstrate the validity of this concept by performing current blockade experiments to capture and detect individual microparticles at Pt microelectrodes using solely the ORR. The readout modality is independent of the absolute O_2 concentration, allowing operation under varying conditions. We further determine how the trajectories of individual microparticles are influenced by the combination of electrophoresis and electroosmotic flows and how these can be utilized to provide continuous detection of cationic particles in water for environmental monitoring.

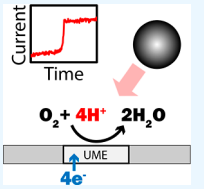

1. INTRODUCTION

Oxygen is the most common oxidant for fuel cell cathodes in sustainable energy technology.[1] While the oxygen reduction reaction (ORR) is omnipresent in energy harvesting technology, it is not as frequently used in electrochemical (bio)sensing. This is despite the fact that the ORR was the key reaction in the first reported biosensor, the glucose sensor,[2,3] in which oxygen consumption by glucose oxidase was monitored to infer glucose concentration.[3] However, due to the stoichiometric limitation of dissolved oxygen (the so-called "oxygen deficit"), oxygen was replaced with synthetic electron acceptors in the next generation of glucose biosensors.[2] Redox mediators such as ferrocene derivatives, ferricyanide, and quinone compounds were employed instead of oxygen as electron acceptor partners.[4] Due to the insensitivity of these mediators to pH, their lower redox potential, and their electrochemically reversible nature, these mediators with outer-sphere electron transfer mechanisms became the conventional species in heterogeneous electron transfer reactions in nearly all amperometric biosensors.[5] ORR has also been used recently as the catalytic reaction in electrochemical immunosensors, where nanostructures that are electroactive for the ORR have been employed as labels for signal amplification[6−16] and for indirect signal generation in surface (bio)sensors.[17−19]

Single-entity electrochemical sensors, like their macroscopic antecedents, often rely on redox species for electron transfer and signal generation.[20,21] Particle impact electrochemistry methods, in particular, employ redox mediators for detecting analytes as discrete events in the current−time response.[21−24] In blockade impact electrochemistry, in particular, the current generated by the flux of mediator to an ultramicroelectrode (UME) is partially blocked by the collision of non-electroactive particles, leading to step-like decreases in the amperometric response.[22] In contrast, in mediated faradaic impact methods, redox mediators undergo oxidation or reduction on the surface of electroactive particles that collide with an otherwise inert UME, leading to amplified current spikes in the current−time response.[23] Redox mediators such as ferrocene derivatives, potassium ferrocyanide, hydrazine, $NaBH_4$, and so forth have been employed in impact measurements for biosensing applications[25−28] and for analyzing electrocatalysts.[29,30] Faradaic impact electrochemistry has been employed to study the ORR at catalysts such as Pt nanoparticles[31−34] and multiwalled carbon nanotubes.[35] Resolving heterogeneity in catalytic activity within nanoparticle populations can be addressed in this manner[31] under different conditions, including alkaline[35] and acidic[33] solutions as well as high pressures.[31]

Here, we employ the ORR in blockade impact electrochemistry for detecting microparticles under physiological salt conditions. Our motivation for employing the ORR is to enable single-entity electrochemical (bio)sensors while sidestepping the undesirable consequences of introducing artificial mediators, which include interference with biochemical processes as well as electrode fouling. We show that the concentration of dissolved oxygen in a physiological buffer (PBS) under ambient conditions is sufficient for signal

Received: May 22, 2023
Accepted: July 25, 2023
Published: August 15, 2023

generation *in vitro* when using a Pt microelectrode. The ORR in fact leads to large mediator currents due to its being a 4-electron reaction and to oxygen's large diffusion coefficient compared to conventional redox mediators. The electric field that is generated by the ORR leads to the migration and collision of positively charged particles on the UME surface that can be observed as discrete blockade signals. As a simple prototypical application, we show here that ultralow concentrations of positively charged microparticles can be detected via ORR-driven blockade impact electrochemistry. This approach is distinct from and complementary to an earlier study of detection based on oxygen-carrying microparticles.[36] Plastic particles are of increasing concern as a health issue: they have been detected in drinking water,[37] and their accumulation and toxicity have been studied in plants,[38] plankton,[39] algae,[40] bacteria,[41] and even in human blood.[42] Among these particles, positively charged microplastics have shown higher cellular uptake, accumulation, and cytotoxicity in comparison to similar negative particles.[43] We further show that by tuning the UME surface, particles can be detected in a dynamic "kiss-and-run" interaction mode rather than permanent adsorption. Through surface functionalization, this approach can be used as a continuous monitoring system for the digital detection of plastic particles in aqueous solutions, such as drinking water. For comparison, we also employ the ORR for detecting Pt nanoparticles via mediated faradaic impact electrochemistry (Supporting Information).

2. RESULTS AND DISCUSSION

2.1. Cyclic Voltammetry. Cyclic voltammetry was performed to evaluate the steady-state limiting current of the ORR on a 10 μm Pt disk UME in PBS buffer (pH 7.4). Depending on the pH of the solution, a direct 4-electron reaction or an indirect peroxide pathway dominates.[44] Figure 1 (black curve) shows the voltammograms for a sweep potential between −0.7 and −0.1 V vs a Pt counter electrode.

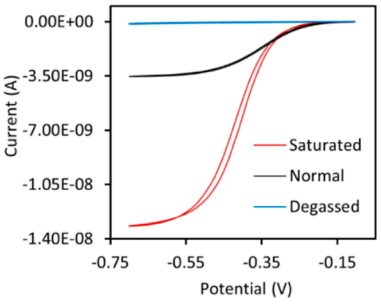

Figure 1. Cyclic voltammograms measured at a Pt disk UME vs Pt wire at a scan rate of 0.05 V/s in PBS (black curve), PBS degassed with N_2 (blue curve), and PBS saturated with pure O_2 (red curve). The potential is applied with respect to a Pt counter electrode in a two-electrode configuration.

The sigmoidal shape of the curve is typical for diffusion-limited transport at a microelectrode, where the limiting current to the UME is given by $I_{lim} = 4nFDCa$. Here, n is the number of transferred electrons, F is the Faraday constant, D is the diffusion coefficient of the reactant at concentration C, and a is the radius of the shrouded disk electrode. The expected limiting ORR current for a diffusion coefficient of O_2 of 2.1 × 10^{-5} cm^2 s^{-1},[45] n = 4, and a concentration of 0.21 mM for water in equilibrium with atmospheric conditions,[31] is $I_{lim} \approx$ 3.4 nA. This compares favorably with the limiting current of ≈3.5 nA obtained from the CV, confirming that the 4-electron reaction ($O_2 + 4H^+ + 4e^- \rightarrow 2H_2O$) is favored in comparison to the indirect two-electron pathway.[31,46] A slight shift in the half-wave potential is also observed, which has been attributed to insufficient buffer capacity when the O_2 concentration becomes too high.[31]

In order to confirm the voltammogram shape and the dependency of the limiting-current level on oxygen concentration, the PBS solution was fed with pure O_2 and degassed with N_2. The red and blue curves in Figure 1 show the increased and decreased limiting-current levels upon oxygen saturation and depletion, respectively. In both measurements, the limiting-current levels returned to their initial values with time in the following cycles through exposure to air as equilibrium was re-established (Supporting Information, Figure S1).

2.2. Blockade Impact Measurements. Blockade impact measurements were performed using a Pt UME biased at negative potentials corresponding to the limiting current. Positively charged 1 μm diameter particles (amidine-modified latex beads, ζ-potential = +32 mV) were used for this measurement. The PBS solution was diluted 25 times in Milli-Q water to decrease the ionic strength. This ensured that the flux of charged particles was dominated by migration instead of diffusion and yielded a high event rate.[21] Reduction of oxygen at the Pt UME generates an electric field with a polarity so as to cause the migration of positively charged particles toward the UME. The arrival of these charged particles at the UME interfered with the mass transport of O_2. Figure 2 presents a typical current−time response for the blockade of the ORR by positively charged microparticles at a potential of −0.7 V vs the Pt counter electrode. Each positive step (decrease in current magnitude) corresponds to a single particle arriving at the electrode.

Due to the independence of the relative step size to the limiting-current level,[22,49,50] the ORR-driven blockade impact is self-calibrating for measurements at different O_2 concentrations. To show the effect of oxygen concentration on the signal-to-noise ratio, impact measurements were performed with oxygen-saturated and partially degassed PBS solutions. As can be seen in Figure 2b,c, $\Delta I/I$ remained essentially unchanged when detecting similar particles in different oxygen concentrations. The independence of the relative signal size on the O_2 concentration means that the ORR-driven blockade impact can also be employed under circumstances where the O_2 concentration is poorly known or varies with time.[51]

2.3. Particle Trajectories. Optical microscopy was performed to analyze the trajectories of the particles. Movies S1 and S2 show the motion of positively charged particles during blockade impact measurements. Charged particles can be seen to move along the surface of the glass shroud and enter the UME area (see also Figure 3a). These trajectories[52] are in the opposite direction from the trajectories for an oxidation reaction (e.g., using a Fc-based mediator), in which particles typically approach the electrode from above (Figure 3b).[53,54] This is attributed to electroosmotic flows (EOF), in which the generation of charged species at the UME induces a tangential electric field that causes electroosmosis in the vicinity of the charged insulating material (glass).[53,54] The fields induced by the oxidation reaction have the opposite polarity from the reduction case, leading to the reversal of both electrophoretic and EOF-induced forces on the particles. At high salt

https://doi.org/10.1021/acsomega.3c03576
ACS Omega 2023, 8, 31265−31270

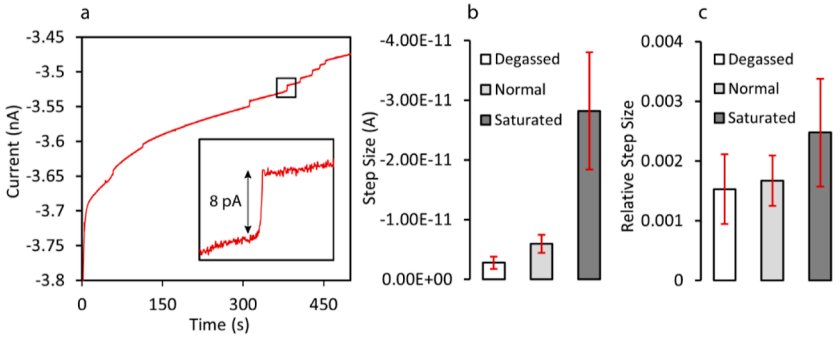

Figure 2. (a) Discrete current steps of blockade of ORR by colliding positively charged particles on a Pt UME when biased at negative potentials in PBS solution diluted 25X in Milli-Q water. (b) Absolute and (c) relative step sizes at different oxygen concentrations (white: partially degassed solution, gray: normal solution, dark gray: oxygen-saturated solution). The error bars represent the standard deviation (10 samples), which originates largely from the inhomogeneous current distribution on the electrode surface.[47,48]

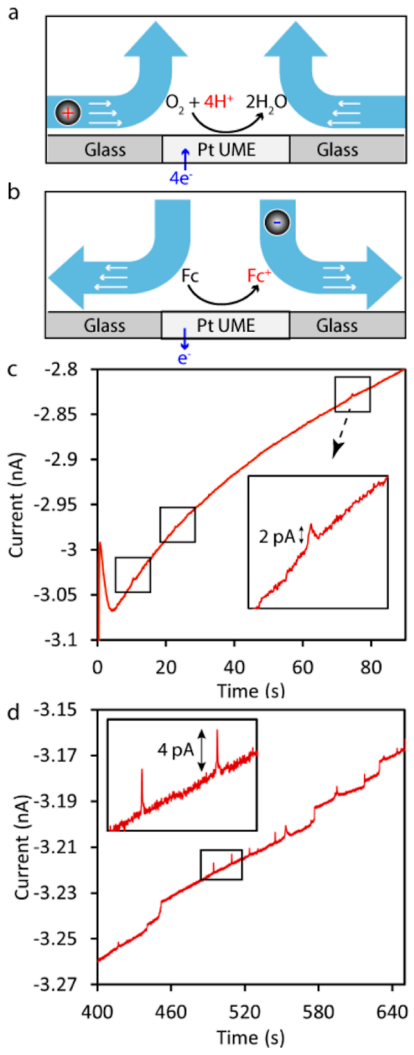

Figure 3. (a, b) Direction of self-induced convection and particle trajectories in reduction (a) and oxidation (b) reactions. (c) Transient amperometric responses upon collision of positively charged particles on a Pt UME surface when biased at negative potentials in a PBS solution-diluted 500× in Milli-Q water. (d) Detection of positively charged particles on a PLL-coated UME via the ORR-driven blockade impact under no-salt conditions.

concentrations (Movie S1), positively charged particles move along the surface and adsorb onto the edge of the UME. This leads to step-like decreases in the current−time response. A consequence of this sort of trajectory is that particles prefer to adsorb near the rim of the disk, where the current density is highest. Hence, collided particles do not rearrange on the UME surface as they do in oxidative systems.[49,55] Employing reductive reactions like ORR may thus decrease errors in particle-counting measurements by suppressing false events caused by the particle rearrangement. We also note that EOF-induced forces could contribute to the rearrangement mechanism for oxidative reactions, but this has not been investigated to date.

At lower concentrations of salt, the EOF becomes more dominant and further affects the particle trajectories. As can be seen in Movie S2 and schematically in Figure 3a, in this case, particles move vertically away from the surface before even reaching the UME area. This behavior causes dip-like transient amperometric responses, which are much smaller than the typical step-like decreases (Figure 3c). In addition to the effect of EOF on the signal size, it can also decrease the frequency of signals when particles are repelled from the surface to such an extent that they become invisible in the current−time response. Hence, EOF may have both an ameliorative effect on particle transport by causing convection and a negative effect by causing some events to be undetectable (Figure 3a). Care must therefore be exerted in this case in particle concentration analysis.

A common limitation of blockade impact methods is that particle adsorption eventually saturates the UME surface, and the UME as a transducing element cannot be used for long-term measurements or continuous monitoring. Under very low salt conditions (PBS diluted 500× in Milli-Q water), the particles do not land on the electrode (Figure 3c), but the resulting small fingerprints in the current−time response are not easily recognizable. This issue can be solved by functionalizing the metal and glass surfaces. Here, we employ a positively charged polyelectrolyte, poly-L-lysin (PLL), to optimize this approach for detecting cationic particles under different salt conditions. PLL can adsorb non-specifically on both metal and glass surfaces, neutralizing the glass and, consequently, diminishing the EOF.[53,54] On the other hand, positively charged particles are electrostatically repelled from the PLL-coated UME when they come in close proximity to the electrode surface. These "kiss-and-run" events can cause blockade spikes in the current−time responses: as can be seen in Figure 3d, amidine-coated microparticles can be kept from remaining on the surface following collisions, leading to

https://doi.org/10.1021/acsomega.3c03576
ACS Omega 2023, 8, 31265−31270

blockade spikes with an amplitude that is 2−4 times that of the ambiguous spike-like events observed in the uncoated case. This simple electrode functionalization can increase the measurement time. With further optimization, we anticipate the possibility of detecting particles (for example, plastic particles in drinking water) in a long-term measurement system with minimized electrode saturation by the target particles.

3. CONCLUSIONS

In summary, our results demonstrate that dissolved oxygen in physiological solutions can serve as an efficient mediator in single-entity electrochemistry. The faster diffusion coefficient of O_2 in comparison to synthetic redox mediators and the transfer of four electrons yield limiting currents in the same range as most outer-sphere mediators. In addition, due to the insensitivity of $\Delta I/I$ to the oxygen concentration, the ORR-driven blockade impact can be used as a self-calibrating system for particle detection at different oxygen concentrations. We showed that this additive-free method can be employed for detecting cationic particles in water and inferred that it can be used for single-entity measurements in solutions such as cell culture media where the addition of synthetic mediators is undesirable. As a disadvantage of this method, at low salt measurements, the consumption of H^+ on the surface increases the local pH at the electrode interface, which is mitigated in a buffer. We anticipate that this method can also be used in the future for detecting particles inside the cell[56] as an *in vivo* single-entity sensor.

4. EXPERIMENTAL SECTION

All measurements were performed using 1 μm-diameter positively charged amidine-coated latex particles (Invitrogen number A37322, with de-ionized water as the medium, ζ-potential = +32 mV). A 10 μm diameter glass-encased Pt UME (BASi/MF-2005) was used for all measurements. Phosphate-buffered saline (PBS, composition: 0.01 M phosphate buffer, 0.0027 M potassium chloride, and 0.137 M sodium chloride, pH 7.4, at 25 °C) was used as the buffer in the measurements (Sigma, P4417). For blockade impact measurements, a constant potential of −0.7 V was applied to the Pt UME with respect to the Pt wire counter electrode (wire diameter 0.20 mm, ≈10 mm length exposed to solution), corresponding to a highly reducing overpotential. The current was monitored using a transimpedance amplifier (Femto, DDPCA-300). A microscope (Zeiss/Axio Scope Vario) with a LD EC "Epiplan-Neofluar" 50×/0.55 DIC M27 objective (parfocal length = 45 mm, free working distance = 9.1 mm) was used for optical microscopy, recording the motion of the particles in two dimensions simultaneously with the amperometric measurement. Poly-L-lysine hydrobromide (Sigma-Aldrich, P7980) was used for surface functionalization (0.1 mg/mL in PBS buffer on a magnet stirrer for 10 min). For mediated faradaic impact measurements (Supporting Information), an 11 μm diameter carbon UME (BASi) and 50 nm Pt particles (locally synthesized) were used for the measurements.

■ ASSOCIATED CONTENT

Supporting Information

The Supporting Information is available free of charge at https://pubs.acs.org/doi/10.1021/acsomega.3c03576.

Adsorption of positively charged particles on the UME surface under low salt conditions (MP4)

Transient collision of positively charged particles on the UME surface under no-salt conditions (MP4)

Description of materials and methods and additional experimental data (PDF)

■ AUTHOR INFORMATION

Corresponding Author

Serge G. Lemay − *Faculty of Science and Technology and MESA+ Institute for Nanotechnology, University of Twente, 7500 AE Enschede, The Netherlands;* orcid.org/0000-0002-0404-3169; Email: s.g.lemay@utwente.nl

Authors

Taghi Moazzenzade − *Faculty of Science and Technology and MESA+ Institute for Nanotechnology, University of Twente, 7500 AE Enschede, The Netherlands;* orcid.org/0000-0002-3908-6062

Jurriaan Huskens − *Faculty of Science and Technology and MESA+ Institute for Nanotechnology, University of Twente, 7500 AE Enschede, The Netherlands;* orcid.org/0000-0002-4596-9179

Complete contact information is available at: https://pubs.acs.org/10.1021/acsomega.3c03576

Notes

The authors declare no competing financial interest.

■ ACKNOWLEDGMENTS

We acknowledge financial support from TopSector High-Tech Systems and Materials in the TKI project "Early cancer diagnostics".

■ REFERENCES

(1) Shao, M.; Chang, Q.; Dodelet, J.-P.; Chenitz, R. Recent Advances in Electrocatalysts for Oxygen Reduction Reaction. *Chem. Rev.* **2016**, *116*, 3594−3657.

(2) Wang, J. Electrochemical Glucose Biosensors. *Chem. Rev.* **2008**, *108*, 814−825.

(3) Yoo, E.-H.; Lee, S.-Y. Glucose Biosensors: An Overview of Use in Clinical Practice. *Sensors* **2010**, *10*, 4558−4576.

(4) Cass, A. E. G.; Davis, G.; Francis, G. D.; Hill, H. A. O.; Aston, W. J.; Higgins, I. J.; Plotkin, E. V.; Scott, L. D. L.; Turner, A. P. F. Ferrocene-mediated enzyme electrode for amperometric determination of glucose. *Anal. Chem.* **1984**, *56*, 667−671.

(5) Frew, J. E.; Hill, H. A. O. Electrochemical Biosensors. *Anal. Chem.* **1987**, *59*, 933A−944A.

(6) Zhang, K.; Dong, H.; Dai, W.; Meng, X.; Lu, H.; Wu, T.; Zhang, X. Fabricating Pt/Sn−In2O3 Nanoflower with Advanced Oxygen Reduction Reaction Performance for High-Sensitivity MicroRNA Electrochemical Detection. *Anal. Chem.* **2017**, *89*, 648−655.

(7) Ge, X.-Y.; Feng, Y.-G.; Cen, S.-Y.; Wang, A.-J.; Mei, L.-P.; Luo, X.; Feng, J.-J. A label-free electrochemical immunosensor based on signal magnification of oxygen reduction reaction catalyzed by uniform PtCo nanodendrites for highly sensitive detection of carbohydrate antigen 15-3. *Anal. Chim. Acta* **2021**, *1176*, 338750.

(8) Li, L.; Liu, X.; Yang, L.; Zhang, S.; Zheng, H.; Tang, Y.; Wong, D. K. Y. Amplified oxygen reduction signal at a Pt-Sn-modified TiO_2 nanocomposite on an electrochemical aptasensor. *Biosens. Bioelectron.* **2019**, *142*, 111525.

(9) Fan, G.-C.; Gu, S.; Zhang, D.; Hu, Z.; Luo, X. Platinum-based nanocomposite as oxygen reduction catalyst for efficient signal amplification: Toward building of high-performance photocathodic immunoassay. *Biosens. Bioelectron.* **2020**, *168*, 112563.

(10) Wang, R.; Feng, J.-J.; Liu, W.-D.; Jiang, L.-Y.; Wang, A.-J. A novel label-free electrochemical immunosensor based on the enhanced catalytic currents of oxygen reduction by AuAg hollow nanocrystals for detecting carbohydrate antigen 199. *Biosens. Bioelectron.* **2017**, *96*, 152−158.
(11) Toyos-Rodríguez, C.; Adawy, A.; García-Alonso, F. J.; de la Escosura-Muñiz, A. Enhancing the electrocatalytic activity of palladium nanocluster tags by selective introduction of gold atoms: Application for a wound infection biomarker detection. *Biosens. Bioelectron.* **2022**, *200*, 113926.
(12) Wang, R.; Wang, A.-J.; Liu, W.-D.; Yuan, P.-X.; Xue, Y.; Luo, X.; Feng, J.-J. A novel label-free electrochemical immunosensor for ultra-sensitively detecting prostate specific antigen based on the enhanced catalytic currents of oxygen reduction catalyzed by core-shell Au@Pt nanocrystals. *Biosens. Bioelectron.* **2018**, *102*, 276−281.
(13) Zhang, J.; Xu, X.; Qiang, Y. Ultrasensitive electrochemical aptasensor for ochratoxin A detection using AgPt bimetallic nanoparticles decorated iron-porphyrinic metal-organic framework for signal amplification. *Sens. Actuators, B* **2020**, *312*, 127964.
(14) Xia, N.; Liu, G.; Zhang, S.; Shang, Z.; Yang, Y.; Li, Y.; Liu, L. Oxidase-mimicking peptide-copper complexes and their applications in sandwich affinity biosensors. *Anal. Chim. Acta* **2022**, *1214*, 339965.
(15) Wang, A.-J.; Zhu, X.-Y.; Chen, Y.; Yuan, P.-X.; Luo, X.; Feng, J.-J. A label-free electrochemical immunosensor based on rhombic dodecahedral Cu3Pt nanoframes with advanced oxygen reduction performance for highly sensitive alpha-fetoprotein detection. *Sens. Actuators, B* **2019**, *288*, 721−727.
(16) Malecka, K.; Ferapontova, E. E. Femtomolar Detection of Thrombin in Serum and Cerebrospinal Fluid via Direct Electrocatalysis of Oxygen Reduction by the Covalent G4-Hemin-Aptamer Complex. *ACS Appl. Mater. Interfaces* **2021**, *13*, 37979−37988.
(17) Zhou, Y.; Chai, Y.; Yuan, R. Highly Efficient Dual-Polar Electrochemiluminescence from Au25 Nanoclusters: The Next Generation of Multibiomarker Detection in a Single Step. *Anal. Chem.* **2019**, *91*, 14618−14623.
(18) Liao, H.; Jin, C.; Zhou, Y.; Chai, Y.; Yuan, R. Novel ABEI/Dissolved O_2/Ag3BiO_3 Nanocrystals ECL Ternary System with High Luminous Efficiency for Ultrasensitive Determination of MicroRNA. *Anal. Chem.* **2019**, *91*, 11447−11454.
(19) Zong, L.-P.; Li, J.; Shu, G.; Liu, X.; Marks, R. S.; Zhang, X.-J.; Cosnier, S.; Shan, D. Rational Design of a Highly Dispersed Fe−N−C Nanosheet with 1,10-Phenanthroline-2,9-Dicarboxylic Acid as a Preorganized Ligand: Boosted Electrochemiluminescence Detection of Tetracycline. *Anal. Chem.* **2022**, *94*, 1325−1332.
(20) Baker, L. A. Perspective and Prospectus on Single-Entity Electrochemistry. *J. Am. Chem. Soc.* **2018**, *140*, 15549−15559.
(21) Moazzenzade, T.; Huskens, J.; Lemay, S. G. Stochastic Electrochemistry at Ultralow Concentrations: the Case for Digital Sensors. *Analyst* **2020**, *145*, 750−758.
(22) Quinn, B. M.; van't Hof, P.; Lemay, S. G. Time-resolved electrochemical detection of discrete adsorption events. *J. Am. Chem. Soc.* **2004**, *126*, 8360−8361.
(23) Xiao, X.; Bard, A. J. Observing single nanoparticle collisions at an ultramicroelectrode by electrocatalytic amplification. *J. Am. Chem. Soc.* **2007**, *129*, 9610−9612.
(24) Sokolov, S. V.; Eloul, S.; Kätelhön, E.; Batchelor-McAuley, C.; Compton, R. G. Electrode−particle impacts: a users guide. *Phys. Chem. Chem. Phys.* **2017**, *19*, 28−43.
(25) Dick, J. E.; Renault, C.; Bard, A. J. Observation of single-protein and DNA macromolecule collisions on ultramicroelectrodes. *J. Am. Chem. Soc.* **2015**, *137*, 8376−8379.
(26) Dick, J. E.; Hilterbrand, A. T.; Boika, A.; Upton, J. W.; Bard, A. J. Electrochemical detection of a single cytomegalovirus at an ultramicroelectrode and its antibody anchoring. *Proc. Natl. Acad. Sci. U.S.A.* **2015**, *112*, 5303−5308.
(27) Dick, J. E.; Hilterbrand, A. T.; Strawsine, L. M.; Upton, J. W.; Bard, A. J. Enzymatically enhanced collisions on ultramicroelectrodes for specific and rapid detection of individual viruses. *Proc. Natl. Acad. Sci. U.S.A.* **2016**, *113*, 6403−6408.
(28) Kwon, S. J.; Bard, A. J. DNA analysis by application of Pt nanoparticle electrochemical amplification with single label response. *J. Am. Chem. Soc.* **2012**, *134*, 10777−10779.
(29) Xiao, X.; Fan, F.-R. F.; Zhou, J.; Bard, A. J. Current Transients in Single Nanoparticle Collision Events. *J. Am. Chem. Soc.* **2008**, *130*, 16669−16677.
(30) Zhou, H.; Fan, F.-R. F.; Bard, A. J. Observation of Discrete Au Nanoparticle Collisions by Electrocatalytic Amplification Using Pt Ultramicroelectrode Surface Modification. *J. Phys. Chem. Lett.* **2010**, *1*, 2671−2674.
(31) Zhang, Y.; Robinson, D. A.; McKelvey, K.; Ren, H.; White, H. S.; Edwards, M. A. A High-Pressure System for Studying Oxygen Reduction During Pt Nanoparticle Collisions. *J. Electrochem. Soc.* **2020**, *167*, 166507.
(32) Li, P.; He, Q.; Liu, H.-X.; Liu, Y.; Su, J.-J.; Tian, N.; Zhan, D. Collision Incidents of Single Tetrahexahedral Platinum Nanocrystals Recorded by a Carbon Nanoelectrode. *ChemElectroChem* **2018**, *5*, 3068−3072.
(33) Xiang, Z.-P.; Tan, A.-D.; Fu, Z.-Y.; Piao, J.-H.; Liang, Z.-X. Oxygen reduction reaction on single Pt nanoparticle. *J. Energy Chem.* **2020**, *49*, 323−326.
(34) Stockmann, T. J.; Angelé, L.; Brasiliense, V.; Combellas, C.; Kanoufi, F. Platinum Nanoparticle Impacts at a Liquid|Liquid Interface. *Angew. Chem., Int. Ed. Engl.* **2017**, *56*, 13493−13497.
(35) Lu, Y.; Li, X.; Compton, R. G. Oxygen Reduction Reaction at Single Entity Multiwalled Carbon Nanotubes. *J. Phys. Chem. Lett.* **2022**, *13*, 3748−3753.
(36) Shimizu, K.; Sokolov, S. V.; Kätelhön, E.; Holter, J.; Young, N. P.; Compton, R. G. In situ Detection of Microplastics: Single Microparticle-electrode Impacts. *Electroanalysis* **2017**, *29*, 2200−2207.
(37) Eerkes-Medrano, D.; Leslie, H. A.; Quinn, B. Microplastics in drinking water: A review and assessment. *Curr. Opin. Environ. Sci. Health* **2019**, *7*, 69−75.
(38) Sun, X.-D.; Yuan, X.-Z.; Jia, Y.; Feng, L.-J.; Zhu, F.-P.; Dong, S.-S.; Liu, J.; Kong, X.; Tian, H.; Duan, J.-L.; Ding, Z.; Wang, S.-G.; Xing, B. Differentially charged nanoplastics demonstrate distinct accumulation in Arabidopsis thaliana. *Nat. Nanotechnol.* **2020**, *15*, 755−760.
(39) Cole, M.; Coppock, R.; Lindeque, P. K.; Altin, D.; Reed, S.; Pond, D. W.; Sørensen, L.; Galloway, T. S.; Booth, A. M. Effects of Nylon Microplastic on Feeding, Lipid Accumulation, and Moulting in a Coldwater Copepod. *Environ. Sci. Technol.* **2019**, *53*, 7075−7082.
(40) Zheng, X.; Liu, X.; Zhang, L.; Wang, Z.; Yuan, Y.; Li, J.; Li, Y.; Huang, H.; Cao, X.; Fan, Z. Toxicity mechanism of Nylon microplastics on Microcystis aeruginosa through three pathways: Photosynthesis, oxidative stress and energy metabolism. *J. Hazard. Mater.* **2022**, *426*, 128094.
(41) Feng, L.-J.; Li, J.-W.; Xu, E. G.; Sun, X.-D.; Zhu, F.-P.; Ding, Z.; Tian, H.; Dong, S.-S.; Xia, P.-F.; Yuan, X.-Z. Short-term exposure to positively charged polystyrene nanoparticles causes oxidative stress and membrane destruction in cyanobacteria. *Environ. Sci.: Nano* **2019**, *6*, 3072−3079.
(42) Leslie, H. A.; van Velzen, M. J. M.; Brandsma, S. H.; Vethaak, A. D.; Garcia-Vallejo, J. J.; Lamoree, M. H. Discovery and quantification of plastic particle pollution in human blood. *Environ. Int.* **2022**, *163*, 107199.
(43) Roshanzadeh, A.; Park, S.; Ganjbakhsh, S. E.; Park, J.; Lee, D.-H.; Lee, S.; Kim, E.-S. Surface Charge-Dependent Cytotoxicity of Plastic Nanoparticles in Alveolar Cells under Cyclic Stretches. *Nano Lett.* **2020**, *20*, 7168−7176.
(44) Yeager, E. Electrocatalysts for O_2 reduction. *Electrochim. Acta* **1984**, *29*, 1527−1537.
(45) Cussler, E. L. *Diffusion: Mass Transfer in Fluid Systems*; Cambridge University Press, 1997.
(46) Kulkarni, A.; Siahrostami, S.; Patel, A.; Nørskov, J. K. Understanding Catalytic Activity Trends in the Oxygen Reduction Reaction. *Chem. Rev.* **2018**, *118*, 2302−2312.

https://doi.org/10.1021/acsomega.3c03576
ACS Omega 2023, 8, 31265−31270

(47) Moazzenzade, T.; Walstra, T.; Yang, X.; Huskens, J.; Lemay, S. G. Ring Ultramicroelectrodes for Current-Blockade Particle-Impact Electrochemistry. *Anal. Chem.* **2022**, *94*, 10168−10174.
(48) Deng, Z.; Elattar, R.; Maroun, F.; Renault, C. In Situ Measurement of the Size Distribution and Concentration of Insulating Particles by Electrochemical Collision on Hemispherical Ultramicroelectrodes. *Anal. Chem.* **2018**, *90*, 12923−12929.
(49) Boika, A.; Thorgaard, S. N.; Bard, A. J. Monitoring the Electrophoretic Migration and Adsorption of Single Insulating Nanoparticles at Ultramicroelectrodes. *J. Phys. Chem. B* **2013**, *117*, 4371−4380.
(50) Bonezzi, J.; Boika, A. Deciphering the Magnitude of Current Steps in Electrochemical Blocking Collision Experiments and Its Implications. *Electrochim. Acta* **2017**, *236*, 252−259.
(51) Lemay, S. G.; Moazzenzade, T. Single-Entity Electrochemistry for Digital Biosensing at Ultralow Concentrations. *Anal. Chem.* **2021**, *93*, 9023−9031.
(52) Weiß, L. J. K.; Music, E.; Rinklin, P.; Banzet, M.; Mayer, D.; Wolfrum, B. On-Chip Electrokinetic Micropumping for Nanoparticle Impact Electrochemistry. *Anal. Chem.* **2022**, *94*, 11600−11609.
(53) Moazzenzade, T.; Yang, X.; Walterbos, L.; Huskens, J.; Renault, C.; Lemay, S. G. Self-Induced Convection at Microelectrodes via Electroosmosis and Its Influence on Impact Electrochemistry. *J. Am. Chem. Soc.* **2020**, *142*, 17908−17912.
(54) Thorgaard, S. N.; Jenkins, S.; Tarach, A. R. Influence of Electroosmotic Flow on Stochastic Collisions at Ultramicroelectrodes. *Anal. Chem.* **2020**, *92*, 12663−12669.
(55) Fosdick, S. E.; Anderson, M. J.; Nettleton, E. G.; Crooks, R. M. Correlated Electrochemical and Optical Tracking of Discrete Collision Events. *J. Am. Chem. Soc.* **2013**, *135*, 5994−5997.
(56) Fu, A.; Yao, B.; Dong, T.; Chen, Y.; Yao, J.; Liu, Y.; Li, H.; Bai, H.; Liu, X.; Zhang, Y.; Wang, C.; Guo, Y.; Li, N.; Cai, S. Tumor-resident intracellular microbiota promotes metastatic colonization in breast cancer. *Cell* **2022**, *185*, 1356−1372.e26.

https://doi.org/10.1021/acsomega.3c03576
ACS Omega 2023, 8, 31265−31270